 FDMP, vol.11, no.3, pp.221-240, 2015

On the Formation Mechanism and Characteristics of High-Pressure Percussion Pulsed Water Jets

Yong Liu[1], **Jianping Wei**[2,3]

Abstract: Although the socalled percussion-pulsed-water jet technique is currently recognized as an effective means for breaking hard rocks, it can't be extensively employed due to insufficient systematic research on the related flow-field structure. Considered as one of the rock breaking technologies with the highest potential of development and application, this method is characterized by water hammer effects, a high-frequency impact pressure and high-speed side flows. The typical (impact and extrusion) pistons used for this technique collide several times to form the multi-pulsed jet. Here we analyze these features through a combined experimental-numerical investigation. The number of pulses and kinetic parameters of the jet are studies as a function of the mass of piston, the speed of the impact piston before collision, the diameter of water chamber, the water depth in the chamber and the nozzle diameter. Interestingly, the jet pressure and velocity first increase from zero and then decrease following a non-linear (quadratic) law. As the mass of the extrusion piston is reduced, the number of pulses increases. We also study in detail the typical umbrella-shaped configuration of the pulsed jet by means of a VOF numerical method. We show the existence of a back jet and a front jet transporting fluid away from the central regions under the action of air friction and resistance. With the loss of acceleration, the jet moves backward giving rise to an umbrella structure. The formation of the umbrella shape is observed to improve the degree of convergence. A low-velocity layer is identified at the front of the jet, where the turbulent kinetic energy is relatively high.

Keywords: Percussion pulsed water jet; flow field; CFD; umbrella structure

[1] State Key Laboratory Cultivation Base for Gas Geology and Gas Control, Henan Polytechnic University, Jiaozuo, China

[2] The Collaborative Innovation Center of coal safety production of Henan Province, Jiaozuo 454000, Henan, China

[3] Corresponding author

1 Introduction

Considered as one of the rock breaking technologies with the highest potential of development and application, high-pressure pulsed water jet is characterized by water hammer effects, high-frequency impact pressure and high-speed side flow, etc, which may damage large scales of rocks step by step when its pressure is higher than the compressive strength and is a hard rock breaking technology with comparatively less energy losses [Carranza-Torresa and Fairhurstb (1980); Foldyna, Sitek, Švehla, and Svehla (2004)]. For percussion pulsed water jet, parameters such as pulse length and frequency are highly controllable, so indirect emission may be realized to effectively avoid the impacts of water cushion and water return inside eroded holes, which may be more convenient for breaking large rocks [Chahine and Courbière (1987); Fukuichi, Abe, and Fujiwara (2009)]. Nonetheless, there is still a lack of systematical studies on the flow field structure of percussion pulsed water jet, as a consequence of which the water jet was restricted from breaking hard rocks. The research on characteristics of flow field structure of water jets has mostly focused on continuous water jets, whereas lessons may be drawn from these research methods in analyzing the flow field structure of percussion pulsed water jet.

The convergence of flow field structure at the nozzle of a continuous jet may be analyzed by experimentally measuring jet pressure at outlet and impact force in combination with shooting pictures, whereas the whole jet flow field and the structure may not be reflected from these jet parameters. Conventional tests may merely measure the value of pressure and impact force at certain point or several points, but can't obtain complete information about jet [Lasheras, Villermaux, and Hopfinger (1998); Shi and Takayama (1999); Shi, Takayama, and Nagayasu (1995)]. With the development of high technologies such as LDA (Laser Doppler Anemometry) and Three-dimensional Particle Image Velocimetry (3D-PIV), the flow field may be continuously tested [David, Jardin, Braud, and Farcy (2012); Hori and Sakakibara (2004); Yang, Zhang, and Kang (2010)], whereas these technologies are inapplicable for jets flowing at a speed higher than 400m/s. In analyzing the flow field structure by mathematical models, it is rather difficult to get solutions due to excessively complicated equations or too many conditional hypotheses, which fail to conform to the real flow structure well [Bloor (1978); Field and Lesser (1977)]. As a crucial tool for researching complex turbulent flow fields, CFD (Computational Fluid Dynamics) plays an important role in studying flow field structure. VOF multiphase flow models and realizable k-ε turbulent models may be used to analyze the impacts of nozzle structure on the evolution of jet flow field [Anantharamaiah, Tafreshi and Pourdeyhimi (2006)], calculate the impact force of jet drops [Tafreshi and Pourdeyhimi (2003)], and simulate drop breakup and atomization processes

caused by shearing instability of short waves at liquid-gas boundary [Srinivasan, Salazar, and Saito (2011)] as well as the structure of continuous water jet and jet velocity distribution, etc [Guha, Barron, and Balachandar (2011)]. CFD has been effectively used for simulating high-velocity jets and solving practical problems.

Compared with continuous water jet, the percussion pulsed water jet is more complex with greater difficulties to be studied, so its flow field structure may be examined by CFD to visualize transient, turbulent and multi-phase flow fields. After comparatively analyzing tests, experiments and theoretical calculations, requisite references and basis may be provided for examining mechanisms about the optimization of jet formation devices and jet-related applications.

Thus, a mathematical difference model was established in this paper to examine the flow field characteristics of percussion pulsed water jet. By experimentally analyzing jet velocity, pressure distribution characteristics and jet formation process, the author studied the effects of different experimental parameters such as chamber length, nozzle diameter and mass of extrusion piston on the characteristics of jet structure. The formation mechanism of umbrella-shaped jet tip and changes of flow field during jet formation were analyzed by CFD, mainly including the changes of eddy size around jet, variation of axial velocity of jet and distribution of turbulent kinetic energy.

2 Experimental Analyses on Flow Field Characteristics of Percussion High-pressure Pulsed Water Jet

2.1 Mathematical Models

Ordinary physical model for the formation of percussion jet is shown in Figure 1 as follows. The impact piston moved at high speed and collided with the stationary extrusion piston. Water was squeezed out of the extrusion chamber and composed high-velocity jet after the extrusion piston gained momentum, while the piston was negatively accelerated to move at an increasingly lower speed. The extrusion piston moving at a decreasing speed may meet again with the impact piston moving behind and collide with each other again. Repetitively, the pistons would collide several times to form multi-pulse jet. Assuming both the piston and the chamber were linear elastic rigid bodies, the number of pulses and changes to kinetic parameters of jet would be primarily correlated to the mass of piston, the speed of the impact piston before collision, the diameter of water chamber, the water depth at chamber and the nozzle diameter. During the jet formation, acoustic energy, heat energy and internal energy will be consumed due to collision, friction, volume losses and elastic deformation of chamber, etc, whereas the consumed energy is comparatively lower than the energy transferred to the water by the piston moving at high speed.

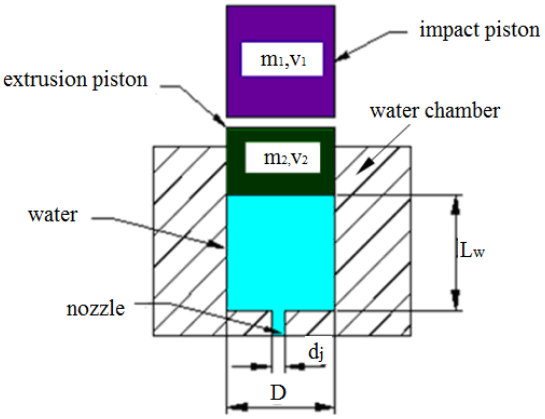

Figure 1: Schematic Diagram for the Formation of Percussion Pulsed Water Jet

The impact extrusion process was generally completed within hundreds of microseconds. Supposing the energy changes weren't affected by power source after the collision between the impact piston and the extrusion piston and the impacts of gravity of two pistons were neglected in the present research, the speed of two pistons after their collision might be derived by energy and momentum conservation laws as follows:

$$v_1 = \frac{2m_2u_2 + u_1(m_1 - m_2)}{m_1 + m_2} \tag{1}$$

$$v_2 = \frac{2m_1u_1 + u_2(m_2 - m_1)}{m_1 + m_2} \tag{2}$$

Where, v_1 is the speed of the impact piston after collision (m/s); v_2 is the speed of the extrusion piston after collision (m/s); u_1 is the speed of the impact piston before collision (m/s); u_2 is the speed of the extrusion piston before collision (m/s); m_1 is the mass of the impact piston (kg); m_2 is the mass of the extrusion piston (kg).

Actually, most collisions aren't absolutely elastic, some of which are transformed into plastic deformation, heat energy and acoustic energy. Thus, formulas (1) and (2) may be modified by a compensation factor. Then, modified equations may satisfy all requirements about non-elasticity and both formulas.

$$v_1 = \frac{(C_R + 1)m_2u_2 + u_1(m_1 - C_Rm_2)}{m_1 + m_2} \tag{3}$$

$$v_2 = \frac{(C_R + 1)m_1u_1 + u_2(m_2 - C_Rm_1)}{m_1 + m_2} \tag{4}$$

Where, C_R is a compensation factor, which may be solved by $C_R = (v_2 - v_1)/(u_1 - u_2)$.

The compensation factor is dependent on physical properties of materials, initial momentum of two collided objects and contacted collision surface, which is characterized by the proportion of speed before and after collision. Elastic collision happened when $C_R = 1$, while both pistons bound together and didn't bounce up.

During collision, the impact piston and the extrusion piston merely collided once when the mass of these two pistons didn't greatly differ from each other. Both pistons would collide multiple times if the mass of the impact piston was much higher than that of the extrusion piston. In this paper, it was defined that these two pistons might collide again when the displacement of the extrusion piston was smaller or equaled to that of the impact piston. Besides, changes occurred to the speed of the impact piston and the extrusion piston, which could be calculated by formulas (3) and (4).

The impacts of the pressure wave inside the chamber may be neglected as well when the chamber diameter is larger than the piston displacement [Rehbinder (1983)]. Assuming the total pressure was the same at all points inside the chamber at the same moment and the effects of nozzle structure on the pressure inside the chamber were neglected, the relationships between the pressure and density inside the chamber might be obtained when $t = t_{i+1}$ based on continuity and momentum equations gained from the jet formation by finite difference method.

$$p_{i+1} = k\frac{\rho_{i+1}}{\rho_i}p_i \tag{5}$$

Where, p_i represents the pressure inside the chamber (Pa); k indicates the bulk modulus of water and 2.2GPa is taken as the constant value.

The density may be calculated according to the mass and the volume of water inside the chamber when $t = t_{i+1}$.

$$\rho_{i+1} = \frac{\rho_i A L_i - \rho_0 (v_j)_{i+1} A_j \Delta t}{A L_{i+1}} \tag{6}$$

Where, L_i is the length of the liquid column inside the chamber at the moment of t_i (m); A_j is the cross-section area of the nozzle (m^2); A is the cross-section area of the chamber (m^2); Δt is the time step (s); and $(v_j)_i$ is the jet velocity at outlet.

The relationships between the water depth at chamber and the time step are obtained as follows:

$$L_{i+1} = L_i - \left((v_p)_i + \frac{p_i A}{m_2} \cdot \Delta t \right) \cdot \Delta t \tag{7}$$

Where, $(v_p)_i$ is the speed of the extrusion piston (m/s).

The difference formula for calculating pressure is obtained from formulas (5), (6) and (7) as follows.

$$p_{i+1} = k\frac{\rho_i A L_i - \rho_0 (v_j)_i A_j \Delta t}{A(L_i - \Delta x_i)\rho_i} p_i \tag{8}$$

Besides, the relationships between the pressure at nozzle and speed are gained from the Bernoulli equation as follows.

$$(v_j)_{i+1} = \sqrt{\frac{2p_{i+1}}{\rho_{i+1}}} \tag{9}$$

Eventually, the following formula is obtained for calculating the speed at nozzle outlet.

$$(v_j)_{i+1} = \sqrt{\frac{2kp_i(\rho_i A L_i - \rho_0 (v_j)_i A_j \Delta t)}{\rho_0 \rho_i A(L_i - (v_{pi} + \frac{p_i A}{m_2})\Delta t)}} \tag{10}$$

2.2 Experimental Settings

The generator of the percussion pulsed water jet is shown in Figure 2, by which the single-pulse jet may be generated with the maximum speed of 600m/s. The speed before the collision between the impact piston and the extrusion piston could be determined pursuant to the initial drop height. The water pressure inside the chamber was measured by a high-precision piezoelectric sensor (PCB108A04), which was placed at the bottom of the chamber. Generated signals were acquired by the digital oscilloscope [Tektronix TDS (2014)] that was connected with the sensor. The formation process of the high-speed percussion impulse water jet was photographed by FASTCAMSA5 high-speed camera at a speed of 20, 000fps and the snapping length of each picture was 100mm.

Experimental parameters are shown in Table 1 as follows. The impact piston was fixed 5.1m high above the impact piston and collided with the extrusion piston at a speed of 10m/s to form a high-pressure percussion pulsed water jet. During the jet formation, pressure signals were acquired inside the digital oscilloscope. Three experiments were conducted under the same working conditions.

2.3 Results and Discussions

Computing programs were written by Matlab to calculate the results at each time step and draw curves for the changes of related parameters with time. Calculated

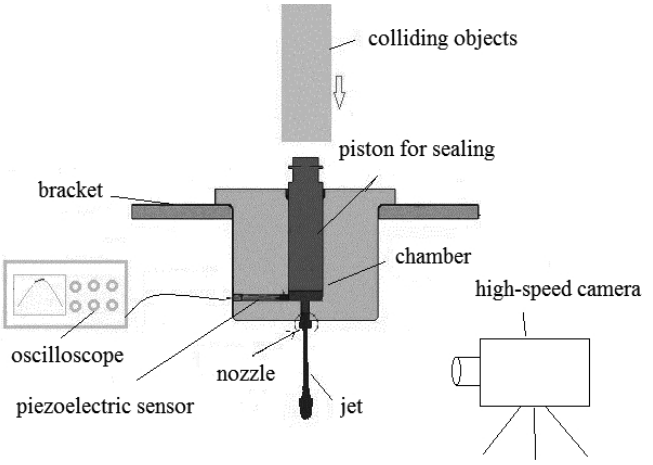

Figure 2: Experimental System for Percussion Pulsed Water Jet

Table 1: Major Working Parameters

Name	Parameters
Mass of Impact Piston	6kg
Mass of Extrusion Piston	2.5kg
Speed of Impact Piston before Collision	10 m/s
Speed of Extrusion Piston before Collision	0 m/s
Chamber Diameter	50mm
Nozzle Diameter	3mm
Water Depth inside Chamber	13mm
Compensation Factor	0.9

structural dimensions and the experimental parameters are shown in Table 1. Initial conditions were $p_0 = 0$, $\rho_0 = 1000\text{kg/m}^3$, $L_0 = 13\text{mm}$ and $v_{p_0} = v_2$ when $t_0 = 0$. Figure 3 shows the changes of the pressure inside the chamber with time, which were highly consistent with the data of three tests under the same experimental conditions. The pressure firstly increased from zero and then declined in the form of parabolic curves several times. Two parabolic curves interacted near 0.23ms. The first peak pressure was about 150MPa and the second peak value was approximately 120MPa, which fell to zero near 0.48ms. The experimental results indicated that the pressure fluctuated apparently on pressure curves, especially in test 3 within the range of 50MPa. Such fluctuations were incurred by the shock waves caused by mechanical waves inside the chamber during collisions [Pianthong, Zakrzewski, and Behnia (2002)]. The impacts of shock waves inside the chamber were neglected in deriving this difference model, so the curves calculated were relatively

smooth. The influences imposed by the jets of these shock waves may be neglected in examining the main flow field characteristics of jets in engineering applications.

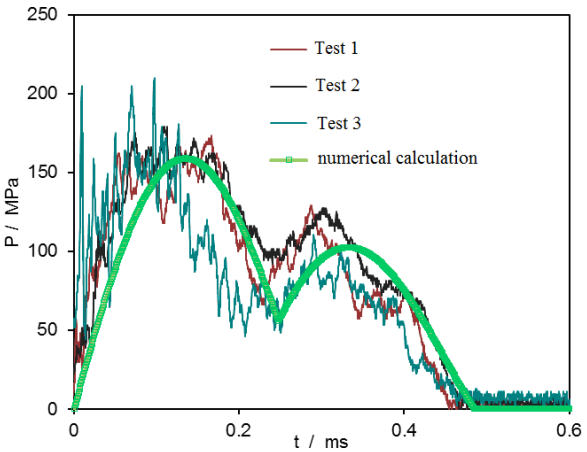

Figure 3: Changes of Water Pressure inside the Chamber with Time

As shown in Figure 4, the jet formation process was photographed by a high-speed camera for the purpose of tracking the changes of high-speed flow during jet formation. During the initial jet formation, the umbrella structure hadn't been apparently formed because a low-velocity zone existed in the jet flow field. A halo structure came into being around the jet at the time point of 150 μs as front jet flew faster than the back jet which subsequently rushed out of the halo structure at high speed and composed a high-velocity region [Carranza-Torresa and Fairhurstb (1980)]. The 2nd pulse was sprayed out of the nozzle at 300 μs while the mathematical difference model built in this paper was validated. The 1st pulse was interrupted after it was fractured at its back part due to the decrease of jet pressure. The generation of the second pulse wasn't affected by the low-velocity region, so the umbrella-shaped head structure was obvious. As indicated from Figure 4, the high-resolution picture clearly showed typical jet structure at the front jet of the 2nd pulse at the time point of 0.4ms.

The mathematical model that has been built may not only predict the changes of jet pressure, but may also forecast the jet velocity at outlet and the motion of the impact piston and the extrusion piston. The curve for jet velocity at outlet (Figure 5) is identical to the pressure curve, which also reflects multiple collisions between the impact piston and the extrusion piston. Within the time range of 0-0.15ms, the jet velocity at outlet tended to sharply increase and the back jet caught up with the front jet and flew faster to form a high-velocity region, while the front low-velocity jet composed a halo region around jet [Carranza-Torresa and Fairhurstb

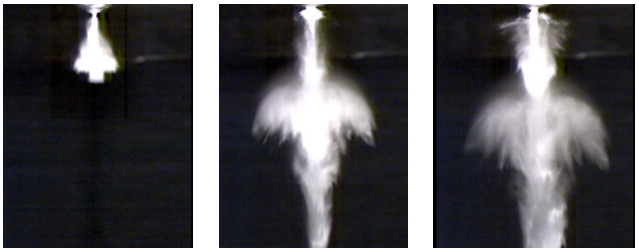

0.15ms 0.3ms 0.4ms

Figure 4: High-resolution Pictures of the Formation Process of Percussion Jet

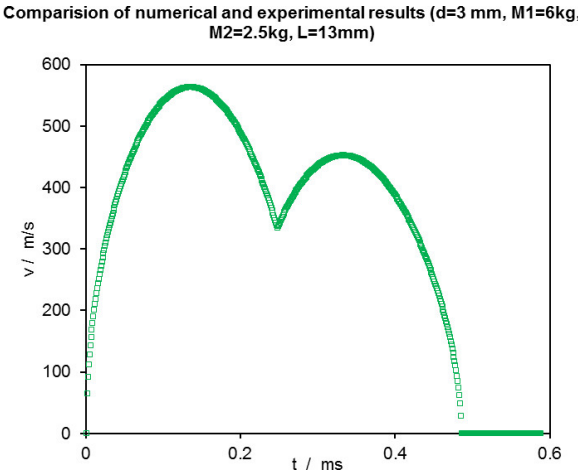

Figure 5: Changes of Jet Velocity at Nozzle Outlet with Time

(1999)]. After the flow of this part of jet, the jet velocity declined within the time range from 0.23 to 1.15ms, as a consequence of which the jet was interrupted and fractured. The 2nd pulse formed because of the acceleration after the time point of 0.23ms.

The calculation results (Figure 6 and 7) mainly indicate the motion of the impact piston and the extrusion piston during jet formation. The first collision happened at 0ms and the extrusion piston was separated from the colliding object after it moved faster than the impact piston and moved on more slowly due to the water resistance inside the chamber. At the time point of 0.17ms, the extrusion piston moved in the opposite direction at an increasingly higher speed. Subsequently, it met the colliding object moving at a constant speed at 0.25ms and collided with each other again. After the second collision, the colliding object was negatively accelerated. As the impact piston was accelerated or stagnant in a direction opposite to the extrusion di-

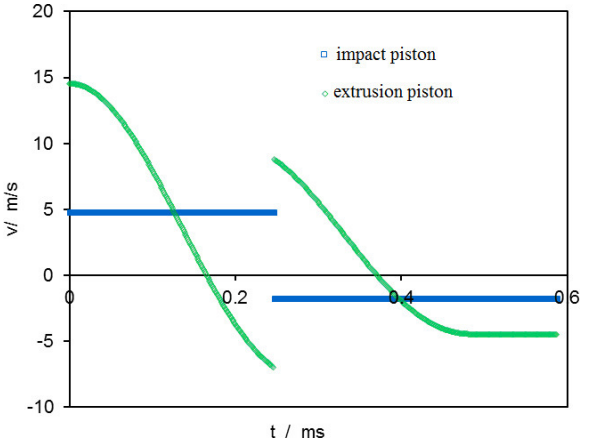

Figure 6: Changes of the Speed of the Impact Piston and the Extrusion Piston with Time

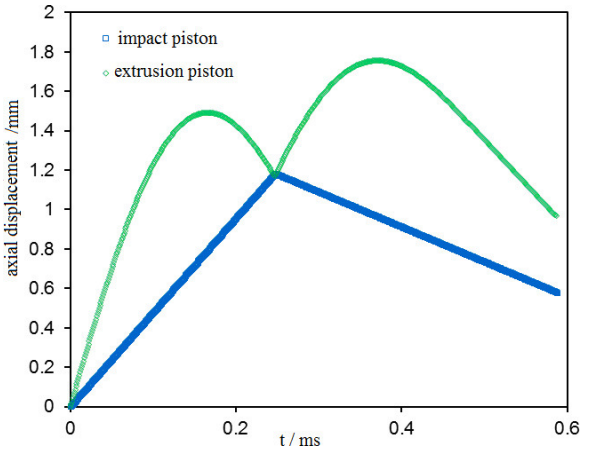

Figure 7: Changes of the Axial Displacement of the Impact Piston and the Extrusion Piston with Time

rection, the extrusion piston slowly became stagnant as the energy was consumed. It can be seen from Figure 7 that the maximum displacement of the extrusion piston is 1.7mm. After reaching the maximum displacement, the extrusion piston moved to the point where $x = 1$mm under the action of water pressure.

2.4 Impacts of Experimental Parameters on Flow Field Structure

To analyze the impacts of different experimental parameters on jet pressure, the changes of chamber pressure with time were examined under the conditions of different water depth at chamber, nozzle diameter and mass of extrusion piston as shown in Figure 8, 9 and 10. It can be found from Figure 8 that jet duration and max jet pressure were determined by the water depth at chamber on the premise that other experimental parameters were known. The higher the water depth at chamber, the longer the jet duration and the lower the max jet pressure. The nozzle diameter exerted similar impacts on jet and water depth at chamber, whereas there were great differences in degree of impacts and change tendency. As the mass of the extrusion piston was reduced, there was an increase in the energy of the single-pulse jet and number of pulses under the action of a single impact. With the increase of pulses, the parabolic increase and decrease on the pressure curve tended to be smoother on the whole.

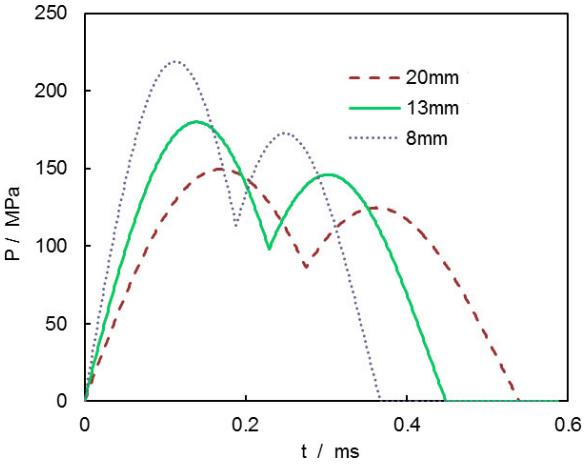

Figure 8: Changes of Pressure with Time at Different Water Depth at Chamber

3 Numerical Analysis on flow Field Structure of Percussion Pulsed Water Jet

In combination with VOF multiphase flow model and realizable k-ε turbulence model, a 2D dynamic transient model was built in this paper and hydrodynamic features of pressure at nozzle outlet was defined by UDF to simulate the formation and structural characteristics of the single-pulse percussion jet. The impacts imposed by the turbulence, shock wave and cavitation effect of the flow field inside the chamber during jet formation were neglected. Considering the drop breakup

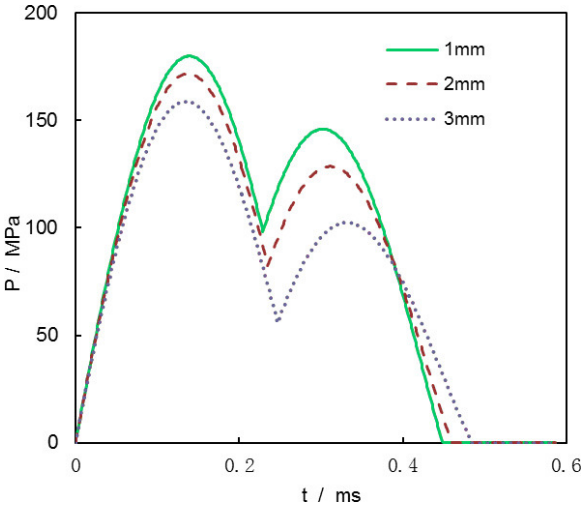

Figure 9: Changes of Pressure with Time under the Conditions of Different Nozzle Diameter

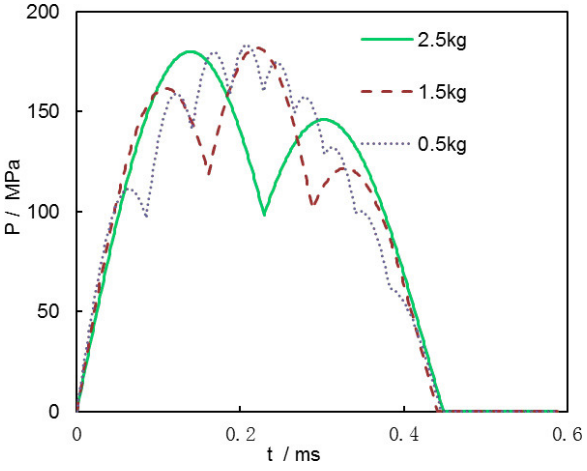

Figure 10: Changes of Pressure with Time under the Conditions of Different Piston Mass

and the atomization at the liquid-gas boundary during jet formation, the author focused on studying the roles of formation mechanism of umbrella-shaped head structure in jet formation.

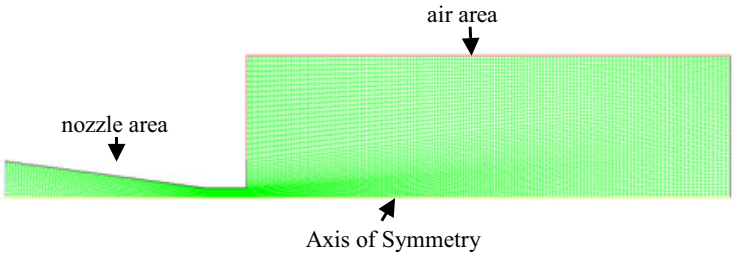

Figure 11: Calculated Areas and Grids

3.1 Grid Partition and Boundary Conditions

A simulation analysis was conducted for the structure of the convergent nozzle with 2mm of nozzle diameter, 13 degree of convergence angle, 30mm of effective length and about 60mm of length in the air area outside the nozzle. The nozzle inlet was the pressure inlet boundary and the changes of the pressure inside the chamber with time were recorded in the UDF to define dynamic features of the transient jet at inlet. Turbulent parameters were determined based on hydraulic radius and turbulent intensity. The relationships of water density with speed of sound and volume modulus were imported to the UDF to define the water compressibility.

3.2 Results and Discussions

To validate the reliability of the calculation model, cloud pictures photographed by a high-speed camera for the jet structure (Figure 12) and simulated volume fraction of fluid (Fig 13) were comparatively analyzed, which showed high similarity. The umbrella-shaped jet initially took shape at the time point of 40 μs, while the thin-layer umbrella structure was gradually broken up as the jet got longer and drops accumulated at the core of jet after breakup. In Fig 14, main characteristic dimensions of two different jet structures were compared. It can be known from the data that the front jet moved ahead nearly in the same direction and the width of the umbrella-shaped jet slightly varied after jet formation. The changes of jet length with time have suggested that front jet velocity tended to be accelerated during jet development. Compared with the experimental pictures, the length and width of the simulated umbrella-shaped jet were slowly narrowed after 160 μs of jet development, because the jet structure was affected by pressure fluctuation and cavitation effect incurred by the shock waves inside the chamber.

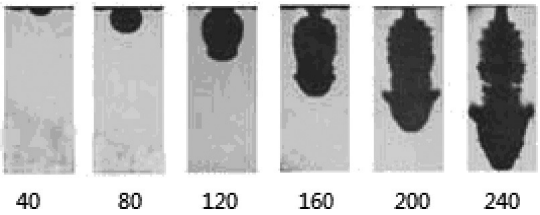

Figure 12: High-resolution Pictures Shot during Jet Formation (μs)

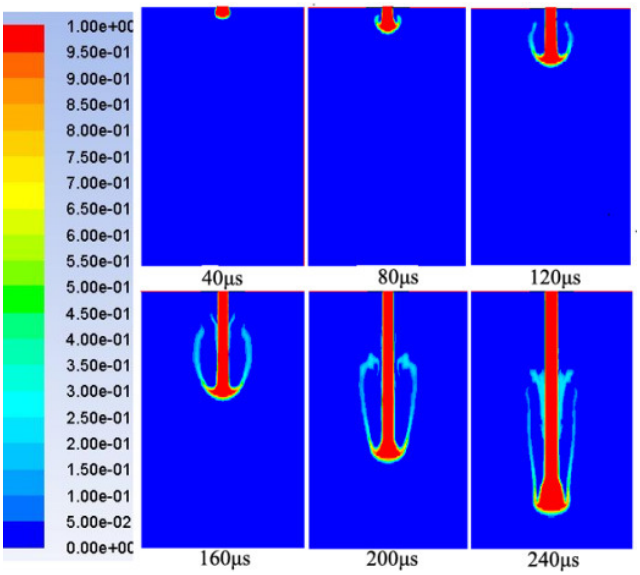

Figure 13: Cloud Picture of Volume Fraction of Jet at Different Moments

3.3 Changes of Flow Field during Jet Formation

The velocity distribution of airflow fields around jet is shown in Figure 15 at the time points of 120 μs and 160 μs. The air moving faster than the jet flew inside the umbrella-shaped zone from the back and turbulent airflow formed due to the limits of surrounding jets. The large eddy at the boundary layer was restricted from expansion since an air layer formed outside the boundary layer of the central jet, which moved faster than the jet towards the same direction. As indicated from Bloor's theoretical research [Bloor (1978)], jet would break up if the eddy size is larger than the effective dimension of the liquid flow after the liquid jet injects into the air. This reflects that the umbrella structure is effective for increasing the degree of convergence for central jets since it restricts the expansion of large eddy with jet.

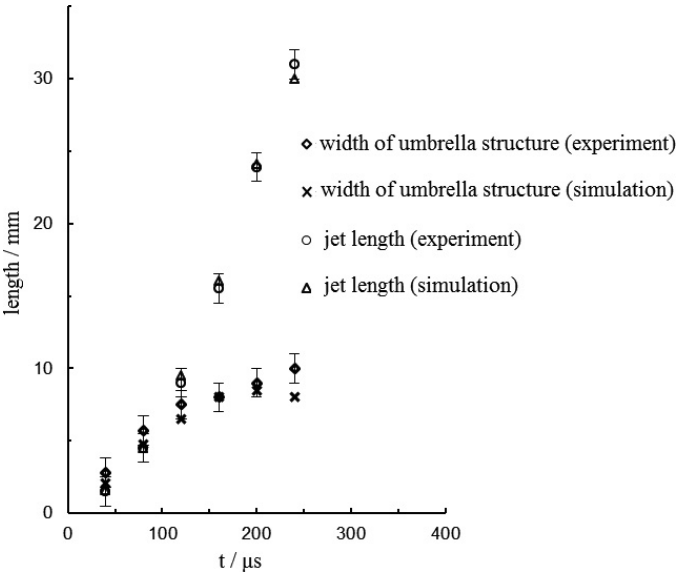

Figure 14: Comparative Analysis on Simulation and Experiment about Structural Dimensions of Jet

In combination with Figure 15 and 16, it may be seen that the liquid layer behind the umbrella structure would be broken up with the expansion of jet and accumulated in the central jet with the entrainment of eddy, which is ascribed to the large eddy size higher than effective dimension of the umbrella-shaped liquid layer, Rayleigh-Taylor instability of high Reynolds number flows and surface tensions, etc [Field and Lesser (1977)].

Figure 17 shows the changes of axial velocity of jet with time. The maximum axial velocity was 50m/s at the time point of 40 μs, while the pressure at the nozzle outlet began to decline at the time point of 240 μs and the front jet had been accelerated to flow at the highest speed. Before the pressure at the nozzle outlet reached the peak, the velocity of the front jet was always lower than that of subsequent jets. The fluid at front jet flew sideways away from the effective core region of jet under the joint action of back jet flowing at higher speed and front air friction & resistance.

After losing the momentum of subsequent fluid, the fluid flowing sideways moved backward from the core region of jet and formed an umbrella-shaped thin-layer hollow structure. Above analysis indicates that the characteristics of a flow field structure are mainly dependent upon hydrodynamic changes of the flow field at nozzle. Theoretically, the jet fully develops at a high velocity at the time point of 240 μs, the axial velocity of which is 480m/s on average. As shown in Figure 18, a

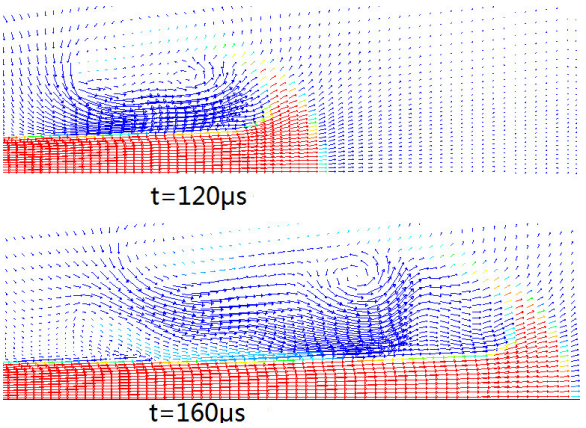

Figure 15: Evolution of Eddy Size around Jet

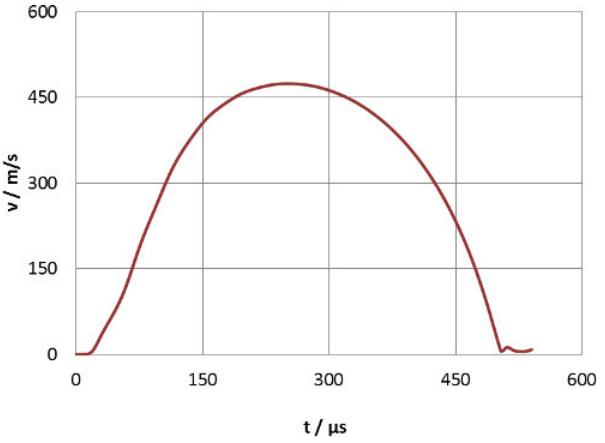

Figure 16: Changes of the Jet Velocity at Nozzle Outlet with Time

layer of low-velocity zone which was nearly twice as thick as the nozzle diameter where the velocity was about 1/2 of the jet velocity at the back effective center formed at the front jet. In addition, the turbulent kinetic energy was fairly high in this zone, which was approximately 1,200 m^2/s^2. This revealed that the extent of pressure fluctuation was large in this zone and "water cushion" was formed for the interaction between the low-velocity head structure and the target in flushing the target, as a result of which the effects of erosion were impacted.

After simulating the jet impingement of a target within 60mm of target range, a curve was obtained for the changes of pressure with time at the central point of

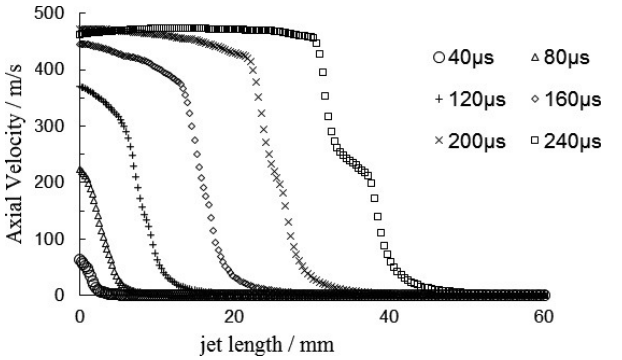

Figure 17: Changes of Axial Velocity during Jet Formation

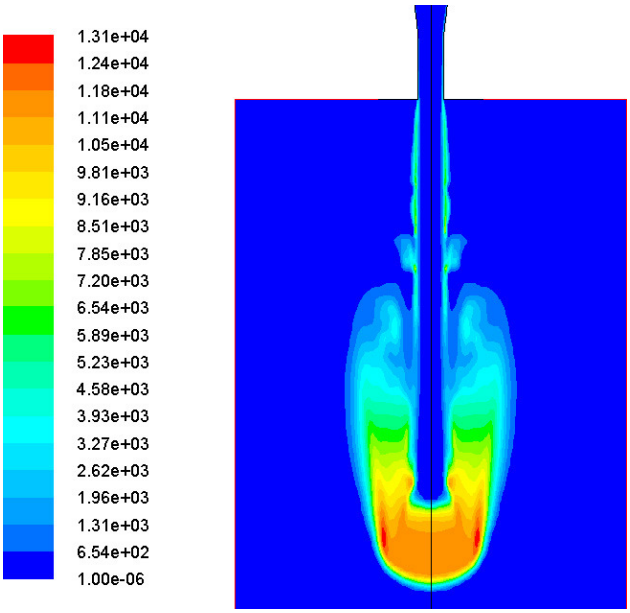

Figure 18: Cloud Image of Turbulent Kinetic Energy of Jet at 240 μs

contact surface of target (Figure 19). Under the initial action of jet, the impact pressure was transformed into the water hammer pressure that was far higher than the stagnation pressure. The water hammer pressure and the duration were connected with the jet head structure and velocity. Compared with the theoretically measured value, the simulated value was smaller and the duration was longer due to the impacts of the jet structure incurred by the effects of air friction & resistance and jet velocity at outlet on jet. The simulation results of jet structure conformed

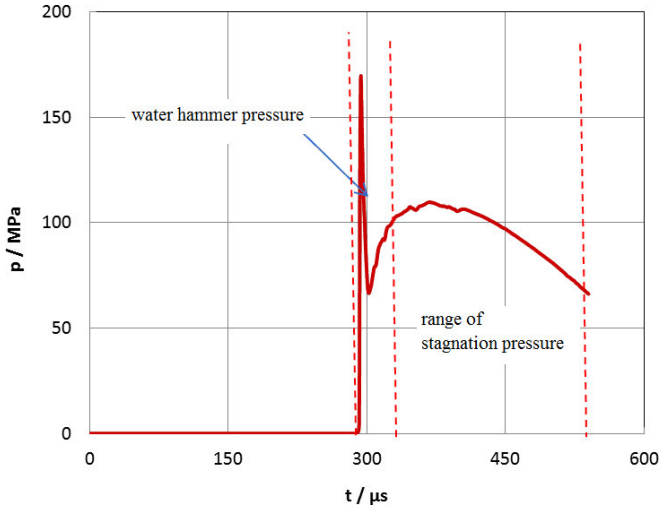

Figure 19: Pressure-time Curve at the Central Point of Jet within 60mm of Target Range

well to real pictures shot by a high-speed camera. This proved that the impact pressure and force calculated by the same model were relatively credible.

4 Conclusions

A mathematical model was elaborated to study the dynamics of a percussion pulsed water jet, able to provide useful information on the changes of jet pressure, velocity at nozzle outlet and the motion of the impact piston and the extrusion piston. The results indicate that the impact piston can collide with the extrusion piston several times, while the pressure inside the chamber has a parabolic increase from zero at the beginning and then a parabolic decrease as time increases. During the first collision, the jet velocity at outlet tends to drastically increase. With the fall of the jet velocity, the high-speed jet formed during the second collision moves faster than the front jet, as a result of which the halo effect is promoted around the jet.

Jet duration and max jet pressure depend of the water depth in the chamber. The higher the water depth, the longer the jet duration and the lower the max jet pressure. The nozzle diameter has a similar influence on the jet. As the mass of the extrusion piston was reduced, we observed an increase in the energy of the single-pulse jet and the number of pulses under the action of a single impact. With the increase of pulses, the parabolic increase and decrease on the pressure curve tended to be generally smoother.

We observed the back jet moving faster than the front jet and the jets essentially moving sideways away from the central regions under the action of air friction and resistance. With the loss of acceleration, the jet moves backward forming an umbrella structure. The formation of the umbrella structure can limit the expansion of a large eddy, but has a beneficial effect on the degree of convergence. We observed a low-velocity layer at the front of jet, where the turbulent kinetic energy was relatively higher.

Acknowledgement: This paper is jointly Supported by Program for Changjiang Scholars and Innovative Research Team in University (IRT1235) and Supported by Scientific Research Foundation of State Key Lab. of Coal Mine Disaster Dynamics and Control (2011DA105287-FW201204).

References

Anantharamaiah, N.; Tafreshi, H. V.; Pourdeyhimi, B. (2006): A study on hydroentangling waterjets and their impact forces. *Exp. Fluids*, vol. 41, pp. 103–113.

Bloor M. (1978): Hypersonic liquid jets. *J. Fluid Mech*., vol. 84, pp. 375–384.

Carranza-Torresa, C.; Fairhurstb, C. (1999): The elasto-plastic response of underground excavations in rock masses that satisfy the Hoek–Brown failure criterion. *Int. J. Rock Mech. Min. Sci.,* vol. 36, pp. 777–809.

Chahine, G. L.; Courbière, P. (1987): Noise and erosion of self-resonating cavitating jets. *J. Fluid. Eng*., vol. 109, pp. 429–435.

David, L.; Jardin, T.; Braud, P.; Farcy, A. (2012): Time-resolved scanning tomography PIV measurements around a flapping wing. *Exp. Fluids.*, vol. 52, pp. 857–864.

Field, J.; Lesser, M. (1977): On the mechanics of high speed liquid jets. *Proc. R. Soc. London, Ser. A.*, vol. 357, pp. 143–162.

Foldyna, J.; Sitek, L.; Švehla, B.; Svehla, S. (2004): Utilization of ultrasound to enhance high-speed water jet effects. *Ultranson Sonochem*, vol. 11, pp. 131–137.

Fukuichi, A.; Abe, Y.; Fujiwara, A. (2009): Study on turbulent behavior of water Jet in supersonic steam injector. *Int. J. Power Energy Syst*, vol. 3, pp. 289–300.

Guha, A.; Barron, R. M.; Balachandar, R. (2011): An experimental and numerical study of water jet cleaning process. *J. Mate.r Process Tech.*, vol. 211, pp. 610–618.

Hori, T.; Sakakibara, J. (2004): High-speed scanning stereoscopic PIV for 3D vorticity measurement in liquids. *Meas. Sci. Technol*., vol. 15, p. 1067.

Lasheras, J.; Villermaux, E.; Hopfinger, E. (1998): Break-up and atomization of a round water jet by a high-speed annular air jet. *J Fluid Mech.*, vol. 357, pp. 351–379.

Pianthong, K.; Zakrzewski, S.; Behnia, M. (2002): Supersonic liquid jets: Their generation and shock wave characteristics. *Shock Waves*, vol. 11, pp. 457–466.

Rehbinder, G. (1983): Investigation of water jet pulses generated by an impact piston. *Appl. Sci. Res.*, vol. 40, pp. 7–37.

Shi, H. H.; Takayama, K.; Nagayasu, N. (1995): The measurement of impact pressure and solid surface response in liquid-solid impact up to hypersonic range. *Wear*, vol. 186, pp. 352–359.

Shi, H. H.; Takayama, K. (1999): Generation of hypersonic liquid fuel jets accompanying self-combustion. *Shock Waves.*, vol. 9, pp. 327–332.

Srinivasan, V.; Salazar, A. J.; Saito, K. (2011): Modeling the disintegration of modulated liquid jets using volume-of-fluid (VOF) methodology. *Appl. Math. Mode.*, vol. 35, pp. 3710–3730.

Tafreshi, H. V.; Pourdeyhimi, B. (2003) The effects of nozzle geometry on water-jet breakup at high Reynolds numbers. *Exp. Fluids*, vol. 35, pp. 364–371.

Yang, M.; Zhang, F.; Kang, C. (2010): Experiment and Numerical Simulation of Free Water Jet by a Central-body Nozzle. *Chinese J. Mech. Eng.*, vol. 23, pp. 797–804.